THE NATURE OF SOLAR POLAR RAYS

JING LI, DAVID JEWITT, AND BARRY LABONTE

Institute for Astronomy, 2680 Woodlawn Drive, Honolulu, HI 96822; jing@ifa.hawaii.edu

ABSTRACT

We use time series observations from the *Solar and Heliospheric Observatory* and *Yohkoh* spacecraft to study solar polar rays. Contrary to our expectations, we find that the rays are associated with active regions on the Sun and are not features of the polar coronal holes. They are extended, hot plasma structures formed in the active regions and projected onto the plane of the sky above the polar coronal holes. We present new observations and simple projection models that match long-lived polar ray structures seen in limb synoptic maps. Individual projection patterns last for at least five solar rotations.

Subject headings: Sun: corona — Sun: UV radiation — Sun: X-rays, gamma rays

1. INTRODUCTION

Polar coronal rays are bright raylike or archlike features first seen above the poles of the Sun during total solar eclipse. They have been described in the literature for at least a century (e.g., Maunder 1901), and they are often considered as features of the solar polar coronal holes. Several studies have been conducted to determine the physical properties of these high-latitude rays (Fisher & Guhathakurta 1995; Guhathakurta, Fisher, & Strong 1996). While the classical literature tends to use the terms "ray" and "plume" interchangeably, the recent studies show that the polar rays have physical properties distinct from those of polar plumes. For example, the polar rays are hotter than the background polar hole gas (2.6×10^6 K vs. 0.7×10^6 K; Guhathakurta et al. 1996), while the plumes "are cooler than the background by up to (but not more than) 30%" (De Forest et al. 1997). The reasons for the differences between polar rays and polar plumes have not yet been closely examined. Here we use time series observations made with the EUV Imaging Telescope (EIT) on the *Solar and Heliospheric Observatory* (*SOHO*) and the Soft X-ray Telescope (SXT) on *Yohkoh* between 1996 and 1999 to study the morphology and time dependence of polar rays.

2. DATA ANALYSIS

The observations are based on extreme-ultraviolet and soft X-ray full-Sun disk images taken by the EIT and SXT instruments on board *SOHO* and *Yohkoh*, respectively. About four EIT images per day from 1996 through 1998 were used in our study. Each EIT image was processed for flat-fielding and filter correction. The processed images were used to build limb synoptic maps. The emissions were extracted around the solar limb 3° wide in polar angle and 0.03 $R_\odot$ in altitude. Successive images provide the time domain for this study, leading to the limb synoptic maps. Figure 1 shows more than 2000 EIT 195 Å (Fe XII) images taken between 1996 January and 1998 June. In this figure, low-temperature areas such as the polar holes appear dark, while high-temperature areas such as active regions are bright. To display both southern and northern polar holes clearly, the range of polar angles (PAs) is extended by 90° from 0°–360° to 0°–450°. We used SXT/*Yohkoh* data in movie form to confirm the distribution of the hot plasma associated with active regions moving across the solar disk.

3. RESULTS

Figure 1 shows a number of noteworthy features. The coronal polar holes appear as dark bands between 150° ≤ PA ≤ 210° and 320° ≤ PA ≤ 390°, extending from day of year (DOY) 0 to about DOY 450. For DOY > 450, the polar holes are filled in by a network of multiply crossing rays. Brighter equatorial gas fills the remaining PAs. An active region (PA ∼ 100° on the east limb and ∼260° on the west limb) persists over 13 full rotations from DOY = 0 to DOY = 360. Fingers of emission encroach from low latitudes on the polar hole boundary. After DOY = 210, these fingers bridge the polar holes, forming a sinusoidal feature that persists for at least five rotations. This is dramatically longer than the ∼20 hr lifetime reported for polar plumes (Llebaria et al. 1998). Sinusoids appear simultaneously in the north and south polar holes. At any given time after DOY ∼ 450, the polar holes are crossed by several overlapping sinusoids, thus making a study of the morphology more difficult. In Figure 2, we enlarge a portion of the limb synoptic map from 210 ≤ DOY ≤ 350 days through EIT 284 Å (Fe XV) in which the ray morphology is particularly clear. The polar ray links successive appearances of the active regions on the east and west limbs and clearly draws a connection between the polar rays and the active regions.

To model the polar ray sinusoids, we consider the apparent sky-plane motion of a radial coronal structure as it is carried round by the solar rotation. The position angle of such a structure is given by

$$\psi = \tan^{-1}\left[\frac{\tan(\theta_0)}{\cos(\alpha)}\right], \qquad (1)$$

where θ_0 is the heliocentric latitude and α is the longitude of the feature measured from the east limb,

$$\alpha = \frac{2\pi}{P(\theta_0)}(t_0 + t). \qquad (2)$$

Here $P(\theta_0)$ is the coronal rotation period at latitude θ_0, t is time, and t_0 is the time when the feature crosses the east limb. In equation (1), we have neglected the effect of the tilt of the solar equator relative to the ecliptic plane. By inspection, we take $P(\theta_0) = 27.5$ days (compatible with independent measurements by Ingester et al. 1999). Equation (1) is plotted on Figure 2 for two sample values $\theta_0 = 10°$ (*dotted curve*) and
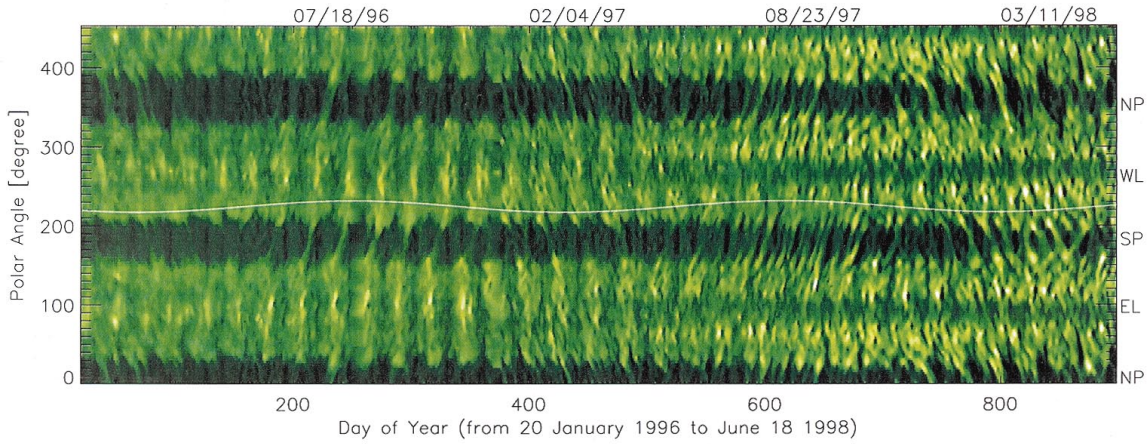
FIG. 1.—Coronal limb synoptic map at 1.0 $R_\odot$ from EIT 195 Å (Fe XII) images in the period from 1996 January to 1998 June. The DOY is indicated along the lower x-axis. The dates are marked along the upper x-axis. The PA is on the y-axis. Zero limb angle corresponds to the north pole (NP), while the east limb is at 90° (EL). To display the entire southern (180°) and northern (0° and 360°) polar holes, the PA is extended by 90°. The heliographic latitude is plotted with a solid curve.

60° (*dashed curve*). The $\theta_0 = 60°$ curve resembles the polar sinusoid rather closely and suggests that this feature is due to a nearly radial coronal ray rooted outside the polar hole but carried across it (in projection) by the solar rotation. Models with $\theta_0 > 60°$, which is the latitude of the boundary of the polar coronal hole at this epoch, do not fit the shapes of the polar sinusoids. The $\theta_0 = 10°$ curve fits the polar sinusoid less well but encompasses a broad swath of near-equatorial emission that is associated with the active regions. Together, the two curves strongly suggest that the polar rays are merely projections of more equatorial gas above the limb of the Sun at high latitudes.

A more detailed but still simplistic three-dimensional corona model was used to test this possibility further. Examination of individual images from EIT and SXT suggested the following representation. We take the active region to be a source of hot gas, which occupies a thick sheet of longitudinal extent $\Delta\alpha$. The boundaries of the region in the meridional plane were assumed to be parabolic with a vertex at the active region. The radial variation of the electron density is assumed to follow

$$n_e(r) = n_{e0}(R_\odot) \exp\left[-\frac{1.5 \times 10^7}{T_e}\left(1 - \frac{R_\odot}{r}\right)\right], \quad (3)$$

which is consistent with hydrostatic equilibrium. We take

$T_e = 2.5 \times 10^6$ K and $n_e(R_\odot) = 3 \times 10^9$ cm^{-3}. The assumption of hydrostatic equilibrium is not critical to our result; any extended distribution of gas that projects above the pole in the plane of the sky gives the same qualitative features. The coronal model outside the active region is taken from our earlier work (Li et al. 2000) and consists of separate parts for the equatorial regions and polar holes. We integrated along the line of sight (including the effects of the tilt of the solar rotation axis) to construct model images of the corona as functions of the solar rotation angle. Figure 3 shows a sample model image in which $\alpha = 30°$. Finally, we constructed limb synoptic maps from the models in the same way as for the data. Examples are shown in Figure 4.

In general, the three-dimensional models behave exactly as expected from simple geometrical considerations (eqs. [1] and [2]). When the heliographic latitude $B_0 = 0$, gas from an active region is visible in projection above the polar holes provided it reaches a radial distance

$$r = \frac{R_\odot}{\sqrt{\cos^2 \theta_0 \cos^2 \alpha + \sin^2 \theta_0}}, \quad (4)$$

where θ_0 is latitude and α is longitude as before. A plasma structure on the meridian ($\alpha = 90°$) at $\theta_0 = 10°$ must extend
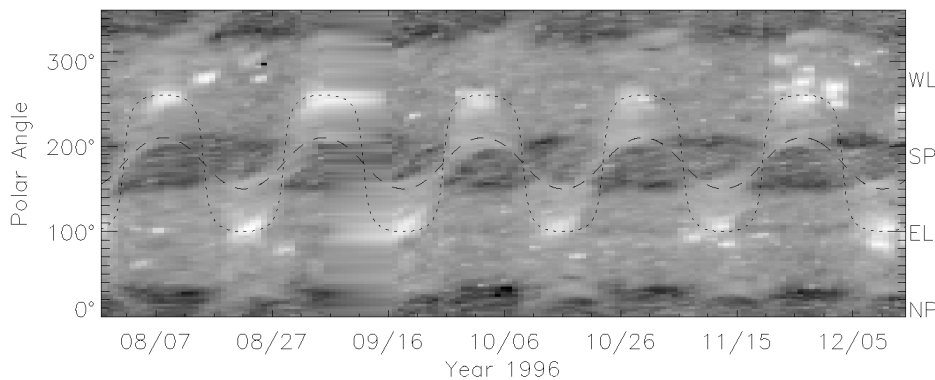

FIG. 2.—A portion of the synoptic chart from EIT 284 Å from DOY = 210 to DOY = 350, corresponding to 1996 July–December. Eq. (1) is plotted for two sample values: $\theta_0 = 60°$ (*dashed curve*) and $\theta_0 = 10°$ (*dotted curve*). The notations on the right side of the figure have the same meaning as those in Fig. 1.
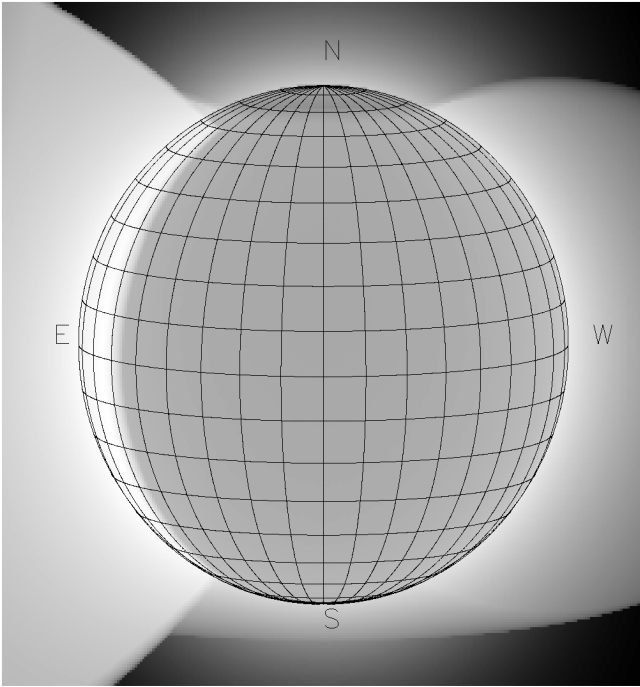
to $r \sim 5.8\,R_\odot$ in order to project above the pole, while a feature at $\theta_0 = 60°$ needs to rise to only $r \sim 1.15\,R_\odot$ in order to be seen. Therefore, the polar rays are most likely the high-latitude edges of extended equatorial structures seen in projection. We used EIT 171 Å (Fe IX, Fe X), 195 Å (Fe XII), and 284 Å (Fe XV) images to estimate the temperatures of the polar rays (e.g., Fig. 1). We find that the rays are hotter than the background polar hole gas, consistent with independent results (Guhathakurta et al. 1996) and with an origin in more nearly equatorial regions. The observation that polar rays appear simultaneously in the north and south holes (see Fig. 1) is naturally explained in this model if the active region is very extended in latitude, consistent with direct images of the active regions when on the solar limb.

Close inspection of the polar sinusoids in Figures 1 and 2 reveals an additional, more subtle long-term variation in morphology. The rising (PA increasing with time) and falling (PA decreasing with time) parts of the polar sinusoids have unequal brightness. In the interval $210 \leq \mathrm{DOY} \leq 350$, the rising branch is systematically brighter than the falling branch, for both northern and southern features. The sense of this asymmetry reverses in the period $350 \leq \mathrm{DOY} \leq 530$ (Fig. 1). In fact, Figure 1 shows that the asymmetry alternates in phase with the heliographic latitude (B_0), suggesting that projection effects are responsible.

Our three-dimensional coronal model, which includes B_0, shows exactly this behavior (see Fig. 4). When the north pole is tilted toward the Earth (Fig. 4, *top*), the model polar rays are brighter on the rising branch than on the falling branch. The opposite pattern is reproduced in the bottom panel of Figure 4 when the north pole is tilted away from the Earth, pro-

FIG. 3.—Sample model image in which the active region is located at 30° longitude and the north pole of the Sun is tilted toward Earth by 7°.25 (i.e., $B_0 = +7°.25$). The image has north to the top, east to the left, and the grid spacing is 10°.
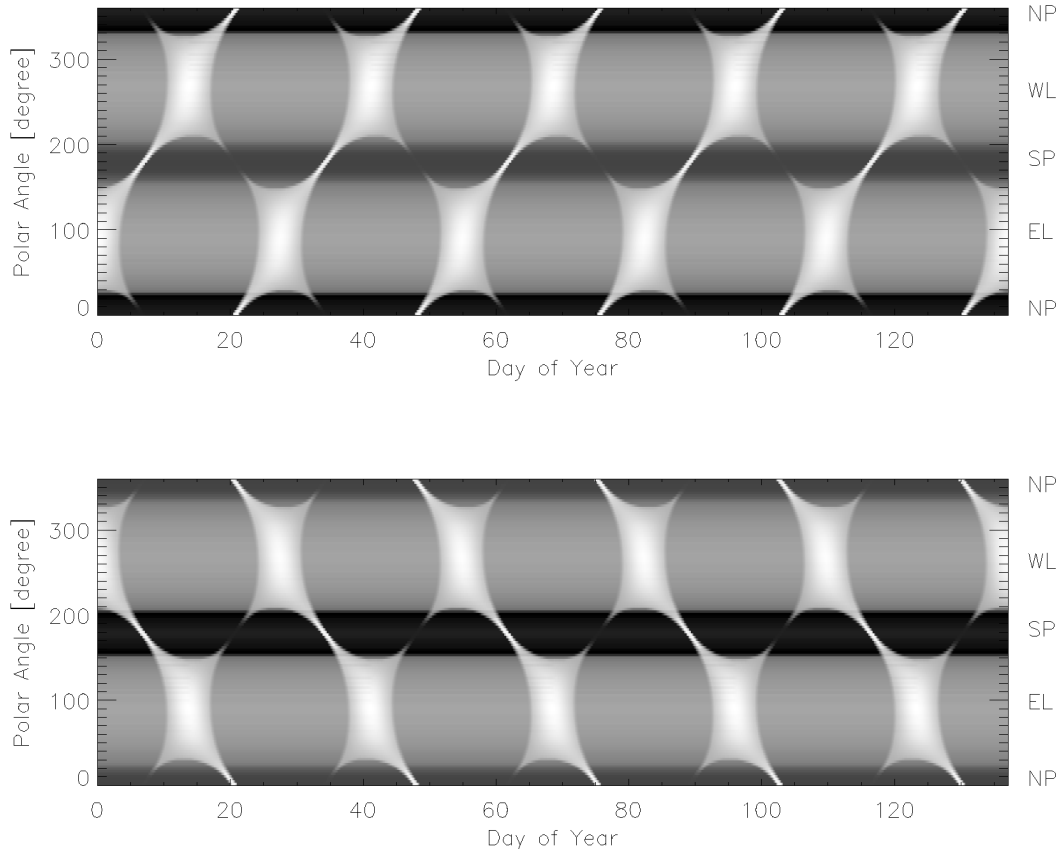

FIG. 4.—Simulated limb synoptic map made from the model of Fig. 3. A rotational resolution of 1° was used. About five solar rotations are included here. *Top*: $B_0 = +7°.25$. *Bottom*: $B_0 = -7°.25$. Note the reversal in the sense of the asymmetry of the brightness of polar rays.

viding a realistic match to the data. When the north pole is tilted toward the Earth, the hot active region gas must rise higher on the far side of the Sun in the southern hemisphere (and on the near side in the north) to meet the line of sight, and so it appears fainter than front-side gas on the line of sight at lower altitudes. Therefore, the bright rising segments near DOY ∼ 242 (see Fig. 2, from 1996 August 23 to September 4) identify an active region on the visible hemisphere of the Sun, as is seen. The periodically reversing brightness asymmetry is a product of projection effects in equatorial plasma.

As the solar cycle approaches its maximum activity, the low-temperature gas in the polar holes is progressively obscured from view by hot equatorial gas projected to high latitudes. This is well seen in Figure 1 where, after DOY ∼ 550, both polar holes are covered by a wormlike network of bright polar rays. The basic morphology of individual rays appears unchanged in the 2.5 years of this study: only the number of polar rays increases toward solar maximum. Some previous reports have claimed that the polar holes vary in size and strength through the solar cycle. Our present results suggest instead that the morphology and visibility of the polar holes are largely controlled by the number and strength of active regions far outside the holes and by the associated high-altitude gas that projects across the holes as polar rays. In future work, we hope to explore this possibility.

4. SUMMARY

1. Limb synoptic maps of the Sun in the period 1996–1998 show long-lived, periodic features in the inner solar corona.

2. Polar rays appear clearly in such maps with a morphology that shows them to be hot gas structures from active regions projected above the polar holes. Unlike polar plumes, which are clearly rooted in the polar coronal holes, the polar rays are not physically associated with the holes.

3. The correlated appearance of polar rays above both north and south holes shows that these features are caused by equatorial plasma structures with a latitudinal extent comparable to the solar diameter.

4. Annually reversing asymmetries in the polar ray brightness on limb synoptic maps are caused by projection effects that are due to the varying heliographic latitude.

5. Individual polar rays are long-lived (more than five rotations in this study) and increase in number as the solar activity cycle approaches solar maximum. The longevity of the polar rays is a reflection of the longevity of active areas that are large enough to be seen in projection above the solar poles.

6. Variations in the visibility of the coronal polar holes are largely controlled by projection of hot gas from more equatorial regions. Polar plumes are features best seen at solar minimum. Polar rays are most prominent near solar maximum.

REFERENCES

De Forest, C. E., Hueksema, J. T., Gurman, J. B., Thompson, B. J., Plunkett, S. P., Howard, R., Harrison, R. A., & Hassler, D. M. 1997, Sol. Phys., 175, 393
Fisher, R., & Guhathakurta, M. 1995, ApJ, 447, L139
Guhathakurta, M., Fisher, R., & Strong, K. 1996, ApJ, 471, L69
Inhester, B., Stenborg, G., Schwenn, R., Srivastava, N., & Podlipnik, B. 1999, Space Sci. Rev., 87, 211

Li, J., Kuhn, J., LaBonte, B., Raymond, J. C., & Acton, L. W. 2000, ApJ, 538, 415
Llebaria, A., Lamy, P., De Forest, C., & Koutchmy, S. 1998, Proc. Int. Meeting on Solar Jets and Coronal Plumes, ed. T. D. Guyenne (ESA SP-421; Noordwijk: ESA), 87
Maunder, E. W. 1901, The Total Solar Eclipse of May 1900 (London: Witherby and Co.)